New Ferrous Complexes Based on the 2,2′-Biimidazole Ligand: Structural, Mössbauer, and Magnetic Properties of $[Fe^{II}(biimH_2)_2(CH_3OH)_2]OAc_2$, $[Fe^{II}(bimH_2)_3]CO_3$, $[Fe^{II}(bimH)_2]_n$, and $\{Fe^{II}(bim)\}_n$

Maria Angeles Martinez Lorente,[†] Françoise Dahan,[†] Yannis Sanakis,[‡] Vasili Petrouleas,[‡] Azzedine Bousseksou,[†] and Jean-Pierre Tuchagues*,[†]

Laboratoire de Chimie de Coordination du CNRS, UP 8241 liée par conventions à l'Université Paul Sabatier et à l'Institut National Polytechnique, 205 route de Narbonne, 31077 Toulouse Cedex, France, and National Research Center "DEMOKRITOS", 153 10 Aghia Paraskevi, Attiki, Greece

Received March 22, 1995[⊗]

Four complexes, $[Fe^{II}(bimH_2)_2(CH_3OH)_2](OAc)_2$ (**1**), $[Fe^{II}(bimH_2)_3]CO_3$ (**2**), $[Fe^{II}(bimH)_2]_n$ (**3**) and $\{Fe^{II}(bim)\}_n$ (**4**), wherein $bimH_2$ = 2,2′-biimidazole, $bimH^-$ = biimidazolate monoanion, and bim^{2-} = biimidazolate dianion, have been synthesized and studied. **1** crystallizes in the monoclinic system, space group $P2_1/n$, $Z = 2$, $a = 9.021(1)$ Å, $b = 7.413(1)$ Å, $c = 17.700(2)$ Å, $\beta = 97.23(1)°$; **2** crystallizes in the tetragonal system, space group $I4_1$, $Z = 4$, $a = b = 12.219(1)$ Å, $c = 14.334(2)$ Å; **3** crystallizes in the tetragonal system, space group $P4_3$, $Z = 4$, $a = b = 8.5144(7)$ Å, $c = 18.273(3)$ Å. The structures were solved by direct methods and refined to conventional agreement indices $R = 0.024$ (**1**), 0.022 (**2**), and 0.032 (**3**) and $R_w = 0.024$ (**1**), 0.023 (**2**), and 0.039 (**3**) with 1725 (**1**), 2292 (**2**), and 2592 (**3**) unique reflections for which $I > 3\sigma(I)$. The molecular structure of **1** consists of $[Fe^{II}(bimH_2)_2(CH_3OH)_2]^{2+}$ complex cations and acetate anions associated into infinite chains along *a* through hydrogen bonds involving the amine nitrogen atoms of all $bimH_2$ ligands, all coordinated methanol molecules and noncoordinated acetate anions. The four nitrogen and two oxygen atoms constituting the distorted coordination octahedron around each Fe(II) originate from two chelating $bimH_2$ ligands and two methanol molecules. The structure of **2** consists of $[Fe^{II}(bimH_2)_3]^{2+}$ complex cations hydrogen bonded to carbonate dianions. The coordination geometry of the iron(II) center can be described as a distorted octahedron includind six nitrogen atoms originating from three chelating $bimH_2$ ligands. The ferrous center of each $[Fe^{II}(bimH)_2]$ neutral unit of **3** is chelated to two biimidazolate monoanions cis to each other. Two deprotonated amine nitrogen donors arising from biimidazolate ligands of adjacent complex molecules supplement the iron(II) coordination octahedron. All iron atoms situated at the same *z* value are bridged through the imidazolate rings affording a sheet spanning along *a,b*. These sheets are associated together into a 3D network in which each $[Fe^{II}(bimH)_2]$ molecule is linked to four nearest neighbors through N−C−N bridges. The synthesis, molecular crystal structure, IR, Mössbauer, and magnetic susceptibility studies of **1**−**4** evidence the variety of structural types and properties obtained for iron(II) complexes of 2,2′-biimidazole and derived biimidazolate anions. Complex **1** is the first example of structurally characterized mononuclear ferrous compound including two bidentate $bimH_2$ and two monodentate oxygenated ligands affording a N_4O_2 coordination sphere to high-spin iron(II). Synthesis of **2** from $Fe^{II}(bimH_2)_2(HCOO)_2$ and CO_3HNa shows that formate anions are readily displaced from the iron(II) coordination sphere as shown for the non-heme iron(II) of photosystem 2. **3** affords the first example of bridging biimidazolate monoanion. **4** is the first inorganic polymeric material including the bim^{2-} dianion as tetradentate bridging ligand. The Mössbauer and magnetic properties of **4** indicate the presence of a weak ferromagnetic ground state resulting from the 3D ordering of this homometallic lattice. **3** and **4** are the first examples of iron compounds including the biimidazolate monoanion ($bimH^-$) and the biimidazolate dianion (bim^{2-}), respectively.

Introduction

We have been involved for several years in the preparation and study of ferrous complexes[1−4] as models of the mononuclear non-heme ferrous site of photosynthetic bacteria[5] and photosystem 2 of oxygenic photosynthetic organisms.[6] One of us has recently shown that the ferrous ion of photosystem 2 is characterized by the presence of a reactive coordination position which can accommodate a number of natural or artificial ligands[7] while numerous authors have proposed the bicarbonate anion HCO_3^- as ligand to the iron alternatively to the glutamate anion of bacterial reaction centers.[6b,8] Thus, our primary goal was to study the reactivity of HCO_3^- with the ferrous ion of previously synthesized model complexes[3] and the competition

* To whom correspondence should be addressed.
[†] Laboratoire de Chimie de Coordination du CNRS.
[‡] Institute of Materials Sciences, NSRC "Demokritos".
[⊗] Abstract published in *Advance ACS Abstracts,* September 15, 1995.

(1) Garge, P.; Padhye, S.; Tuchagues, J.-P. *Inorg. Chim. Acta* **1988**, *157*, 239.
(2) Garge, P.; Chikate, R.; Padhye, S.; Savariault, J.-M.; de Loth, P.; Tuchagues, J.-P. *Inorg. Chem.* **1990**, *29*, 3315.
(3) Boinnard, D.; Cassoux, P.; Petrouleas, V.; Savariault, J.-M.; Tuchagues, J.-P. *Inorg. Chem.* **1990**, *29*, 4114.
(4) Rakotonandrasana, A. S.; Boinnard, D.; Petrouleas, V.; Cartier, C.; Verdaguer, M.; Savariault, J.-M.; Tuchagues, J.-P. *Inorg. Chim. Acta* **1991**, *180*, 19.
(5) Clayton, R. K. *Photosynthesis Physical Mechanisms and Chemical Patterns*; IUPAB-Biophysics Series; Cambridge University Press: Cambridge, England, 1980.
(6) (a) Nugent, J. H. A.; Diner, B. A.; Evans, M. C. W. *FEBS Lett.* **1981**, *124*, 241. (b) Petrouleas, V.; Diner, B. A. *FEBS Lett.* **1982**, *147*, 111. (c) Petrouleas, V.; Diner, B. A. Advances in Photosynthesis Research. In *Proc. Int. Congr. Photosynth., 6th.*, **1984**, *1*, part 2, 195. (d) Rutherford. W.; Zimmermann, J. L. *Biochim. Biophys. Acta* **1984**, *767*, 168. (e) Petrouleas, V.; Diner, B. A. *Biochim. Biophys. Acta* **1986**, *849*, 264.

0020-1669/95/1334-5346$09.00/0

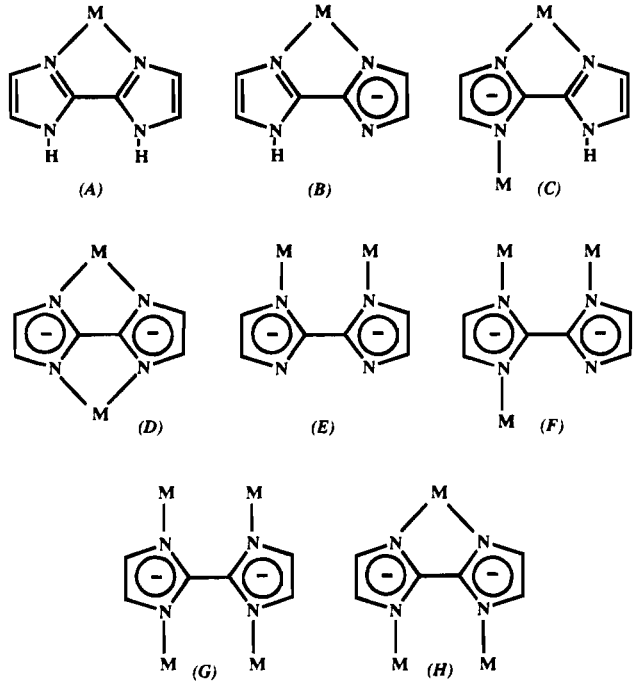

Figure 1. Schematic representation of the possible coordination modes for 2,2′-biimidazole and its mono- and dianions.

reaction between bicarbonate and the anions initially present in these precursors. With the exception of the nucleophylic fixation of CO_2 by hydroxo metal complexes to afford metal bicarbonate or carbonate species,[9] few reactions between preformed metal complexes and bicarbonate (or carbonate) have been described. They involve cobalt(III) or iron(III) precursors and most often bicarbonate and yield cobalt(III) compounds with monodentate[10a] or bridging bidentate[10b] carbonate ligands or polynuclear ferric compounds with μ-CO_3 ligands.[11] It is also worth noticing that, except for the previously mentioned ferrous ion of photosystem 2, the only metalloproteins including a related moiety are transferrins in which a carbonate dianion is chelated to the ferric center.[12] It was thus particularly interesting to explore the reactivity of bicarbonate and carbonate anions with iron(II) with the aim to model the ligand environment of the ferrous ion of photosystem 2 and also to expand the limited knowledge concerning the reactions afforded by these anions with transition metal compounds.

The 2,2′-biimidazole molecule included as a bidentate neutral ligand ($bimH_2$) in the coordination sphere of the iron(II) precursor chosen for these investigations can act as a bi-, tri- or tetra-dentate ligand depending upon its protonation state, *i.e.* neutral biimidazole ($bimH_2$), biimidazolate monoanion ($bimH^-$), biimidazolate dianion (bim^{2-}). Figure 1 shows the different coordination modes that can be afforded by this ligand according to its protonation state. The described metal complexes with either 2,2′-biimidazole or the related 2,2′-bibenzimidazole ligand experiencing the represented (A−H) coordination modes include the following metal ions: (A) M = Rh(I),[13] Cu(II),[14-16] Co(II),[14,16,17] Fe(II),[3,14,16] Fe(III),[16,18] Ni(II),[14,16,17,19] Mo(II),[20] Ru(II);[21] (B) M = Rh(I), Ir(I);[22] (D) M = M′ = Rh(I), Ir(I),[22,23] Mo(II),[20] Ti(III),[24] Co(II),[16] Ni(II),[16] Cu(II),[25] Pd(II),[26] Ru(II),[21,27] Os(II),[27] Mn(II)[28] and M = Ru, M′ = Os;[27] (E−G) M = Au(I);[29] (H) M = M′ = Rh(I)[25] and M = Pd(II), M′ = Au(I).[29] This survey of literature shows that (i) concerning the A coordination mode, there are no structurally characterized ferrous compounds of the $[Fe^{II}(LH_2)_2]X_2$ type, (ii) all described complexes of the $bimH^-$ monoanion are mononuclear, *i.e.*, there is no example of the C coordination mode, (iii) the complexes in which the bim^{2-} dianion exhibits the D coordination mode are dinuclear, and (iv) there is no example of iron compound including either the biimidazolate monoanion ($bimH^-$) or the biimidazolate dianion (bim^{2-}). Considering the basicity of HCO_3^- and CO_3^{2-}, the reaction of bicarbonate or carbonate with iron(II) compounds including the $bimH_2$ ligand was also expected to yield information about the unexplored field of the iron(II) compounds of biimidazolate anions.

In this paper, we report the synthesis and IR, Mössbauer, and variable-temperature magnetic susceptibility results for $[Fe^{II}(bimH_2)_2(CH_3OH)_2](OAc)_2$ (**1**), $[Fe^{II}(bimH_2)_3]CO_3$ (**2**), $[Fe^{II}(bimH)_2]_n$ (**3**), and $\{Fe^{II}(bim)\}_n$ (**4**). X-ray crystal structure determinations of **1**, **2**, and **3** have been performed with the aim to give a detailed interpretation of their Mössbauer and magnetic properties.

Experimental Section

Materials. All reagents were of analytical grade and used without further purification. Solvents were degassed under vacuum prior to

(7) (a) Petrouleas, V.; Diner, B. A. *Biochim. Biophys. Acta* **1990**, *1015*, 131. (b) Diner, B. A.; Petrouleas, V. *Biochim. Biophys. Acta* **1990**, *1015*, 141. (c) Koulougliotis, D.; Kostopoulos, T.; Petrouleas, V.; Diner, B. A. *Biochim. Biophys. Acta* **1993**, *1141*, 275. (d) Deligiannakis, Y.; Petrouleas, V.; Diner, B. A. *Biochim. Biophys. Acta* **1994**, *1188*, 260. (e) Petrouleas, V.; Deligiannakis, Y.; Diner, B. A. *Biochim. Biophys. Acta* **1994**, *1188*, 271.
(8) (a) Dutton, P. L.; Leigh, J. S, Reed, D. W. *Biochim. Biophys. Acta* **1973**, *212*, 654. (b) Diner, B. A.; Petrouleas, V. *Biochim. Biophys. Acta* **1987**, *895*, 107. (c) Robinson, H. H.; Eaton-Rye, J. J.; Van Rensen, J. J. S.; Govindjee, R. *Z. Naturforsch.* **1984**, *39C*, 382. (d) Eaton-Rye, J. J.; Govindjee, R. *Biochim. Biophys. Acta* **1988**, *935*, 248. (e) Nugent, J. H. A.; Corrie, A. R.; Demetriou, C.; Evans, M. C. W.; Lockett, C. J.; *FEBS Lett.* **1988**, *235*, 71. (f) Vermaas, W. F. J.; Rutherford, A. W. *FEBS Lett.* **1984**, *175*, 243. (g) Petrouleas, V.; Diner, B. A. *Biochim. Biophys. Acta* **1987**, *893*, 126.
(9) (a) Rawle, S. C.; Harding, C. J.; Moore, P.; Alcock, N. W. *J. Chem. Soc., Chem. Commun.* **1992**, 1701. (b) Kitajima, N.; Hikichi, S.; Tanaka, M.; Moro-oka, Y. *J. Am. Chem. Soc.* **1993**, *115*, 5496 and references therein.
(10) (a) Churchill, M. R.; Harris, G. M.; Lashewycz, R. A.; Dasgupta, T. P.; Koshy, K. *Inorg. Chem.* **1979**, *18*, 2290. (b) Sadler, G. G.; Dasgupta, T. D. *Inorg. Chim. Acta* **1989**, *167*, 233.
(11) (a) Norman, R. E.; Holz, R. C.; Menage, S.; O'Connor, C. J.; Zhang, J. H.; Que, L. *Inorg. Chem.* **1990**, *29*, 4629. (b) Drüeke, S.; Wieghardt, K.; Nuber, B.; Weiss, J. *Inorg. Chem.* **1989**, *28*, 1414. (c) Jameson, D. L.; Xie, C. L.; Hendrickson, D. N.; Potenza, J. A.; Schugar, H. J. *J. Am. Chem. Soc.* **1987**, *109*, 740.
(12) (a) Baker, E. N.; Anderson, B. F.; Baker, H. M.; Haridas, M.; Norris, G. E.; Rumball, S. V.; Smith, C. A. *Pure Appl. Chem.* **1990**, *62*, 1067. (b) Eaton, S. S.; Dubach, J.; Eaton, G. R.; Thurman, G.; Ambruso, D. R. *J. Biol. Chem.* **1990**, *265*, 7138. (c) Dubach, J.; Gaffney, B. J.; More, K.; Eaton, G. R.; Eaton, S. S. *Biophys. J.* **1991**, *59*, 1091.
(13) Uson, R.; Gimeno, J.; Oro, L. A.; Valderrama, M.; Sariego, R.; Martinez, E. *Transition Met. Chem. (Weinheim, Ger.)* **1981**, *6*, 103.
(14) Holmes, F.; Jones, K. M.; Torrible, E. G. *J. Chem. Soc.* **1961**, 4790.
(15) Sakaguchi, U.; Addison, A. K. *J. Chem. Soc., Dalton. Trans.* **1979**, 600.
(16) Abushamleh, A. S.; Goodwin, H. A. *Aust. J. Chem.* **1979**, *32*, 513.
(17) Nikolenko, L. N.; Tolmacheva, N. S.; Semenova, M. N.; Babievskaya, I. Z.; Kotkova, G. V.; Teterin, A. Y. *Koord. Khim.* **1975**, *1*, 1054.
(18) Dance, I. G.; Abushamleh A. S.; Goodwin, H. A. *Inorg.Chim. Acta* **1980**, *43*, 217.
(19) Mighell, A. D.; Reinmann, C. W.; Mauer, F. A. *Acta. Crystallogr.* **1969**, *25B*, 60.
(20) Calhorda, M. J.; Dias, A. R. *J. Organomet. Chem.* **1980**, *197*, 291.
(21) Rillema, P. D.; Sahai, R.; Matthews, Ph.; Edwards, A. K.; Shaver, R. J.; Morgan, L. *Inorg. Chem.* **1990**, *29*, 167.
(22) (a) Kaiser, S. W.; Saillant, R. B.; Butler, W. M.; Rasmussen, P. G. *Inorg. Chem.* **1976**, *15*, 2681. (b) Kaiser, S. W.; Saillant, R. B.; Butler, W. M.; Rasmussen, P. G. *J. Am. Chem. Soc.* **1975**, *97*, 425.
(23) Kaiser, S. W.; Saillant, R. B.; Butler, W. M.; Rasmussen, P. G. *Inorg. Chem.* **1976**, *15*, 2688.
(24) Fieselman, B. F.; Hendrickson, D. N.; Stucky, G. *Inorg. Chem.* **1978**, *17*, 2078.
(25) Haddad, M. S.; Hendrickson, D. N. *Inorg. Chem.* **1978**, *17*, 2622.
(26) Uson, R.; Gimeno, J.; Fornies, J.; Martinez, F. *Inorg. Chim. Acta* **1981**, *50*, 173.
(27) Haga, M.; Bond, A. M. *Inorg. Chem.* **1991**, *30*, 475.
(28) Uson, R.; Gimeno, J. *J. Organomet. Chem.* **1981**, *220*, 173.
(29) Uson, R.; Gimeno, J.; Fornies, J.; Martinez, F.; Fernandez, C. *Inorg. Chim. Acta* **1981**, *54*, L95.

use. Ferrous acetate and ferrous formate were prepared as previously reported.[3] Due to the high reactivity of iron(II) salts and complexes with dioxygen, complexes were prepared under a purified nitrogen atmosphere in Schlenk-type vessel or in an inert-atmosphere box (Vacuum Atmospheres HE 43-2) equipped with a dry-train (Jahan EVAC 7).

Ligand. 2,2′-Biimidazole ($bimH_2$) was prepared by reaction of aqueous glyoxal (20%) with ammonia, according to the literature method.[24]

$[Fe^{II}(bimH_2)_2(CH_3OH)_2](OAc)_2$ (1). $Fe(CH_3CO_2)_2{\cdot}2H_2O$ (10^{-3} mol) dissolved in 10 mL of deoxygenated methanol was slowly added to a stirred oxygen-free suspension of 2×10^{-3} mol of $bimH_2$ in 30 mL of methanol in an inert-atmosphere box, affording a progressive solubilization of the ligand. The microcrystalline white compound **1** precipitated out of the reaction mixture within 48 h and was filtered off, washed with methanol and dried under vacuum. Yield : 50%. Anal. Calcd for $FeC_{16}H_{18}N_8O_4{\cdot}2CH_3OH$: C, 42.70; H, 5.14; N, 22.14; Fe, 11.04. Found: C, 41.84; H, 5.04; N, 22.27; Fe, 10.89. The resulting dried microcrystalline compound is moderately sensitive to dioxygen.

Colorless crystals of **1** suitable for X-ray measurements were obtained by slow concentration (48 h) of a deoxygenated methanolic solution of **1** (5×10^{-6} mol in 6 mL).

$[Fe^{II}(bimH_2)_3]CO_3$ (2). Procedure a. A deoxygenated glycerol/methanol (1:1) pale yellow solution (40 mL) of $Fe^{II}(bimH_2)_2(HCOO)_2$[3] ($7.5 \times 10^{-4}$ mol) was slowly added to 2×10^{-3} mol of sodium bicarbonate dissolved in 30 mL of an oxygen-free glycerol/water (2:1) mixture. The resulting reaction medium was stirred for three weeks in a purified nitrogen atmosphere, during which the resulting complex slowly precipitated as a microcrystalline yellow-green solid. The complex was filtered, washed with methanol and dried under vacuum. Yield: 47%. Anal. Calcd for $FeC_{19}H_{18}N_{12}O_3{\cdot}CH_3OH$: C, 43.65; H, 4.00; N, 30.55; Fe, 10.16. Found: C, 43.59; H, 4.08; N, 30.43; Fe, 9.79. The reaction time is a very important parameter in this reaction as we have observed that when the precipitate is collected after a shorter period the resulting compound is a mixture of complex **2** (major component) and a second species which is probably $Fe^{II}(bimH_2)(CO_3){\cdot}x$MeOH. For example, a 48 h reaction time affords a mixture including 60% of **2** and 40% of the minor component according to Mössbauer spectrometry.

Pale yellow-green single crystals of **2** suitable for X-ray diffraction studies were obtained by very slow interdiffusion (6 months) between a deoxygenated glycerol/methanol (1:1) solution (45 mL) of $Fe^{II}(bimH_2)_2(HCOO)_2$[3] ($2 \times 10^{-3}$ mol) and a deoxygenated glycerol/ water (2:1) solution (45 mL) of sodium bicarbonate (1.4×10^{-3} mol).

Procedure b. An oxygen-free methanolic solution (2 mL) of $Fe(ClO_4)_2{\cdot}6H_2O$ (7.1×10^{-4} mol) was slowly added to a stirred deoxygenated methanolic suspension (6 mL) of $bimH_2$ (2.14×10^{-3} mol) affording a reddish-brown solution. A deoxygenated glycerol/ water (2:1) solution (30 mL) of sodium bicarbonate (6.3×10^{-3} mol) was then slowly added to the stirred reddish-brown solution. The resulting mixture was stirred for 4 days under a purified nitrogen atmosphere, during which the reddish-brown solution turned yellow and the desired complex progressively precipitated as a yellow-green microcrystalline solid. It was filtered off, washed with methanol, and dried under vacuum. Yield: 70%. Anal. Calcd for $FeC_{19}H_{18}N_{12}O_3{\cdot}CH_3OH$: C, 43.65; H, 4.00; N, 30.55; Fe, 10.16. Found: C, 43.69; H, 3.92; N, 30.53; Fe, 9.66. The resulting dried microcrystalline compound is moderately sensitive to dioxygen.

$[Fe^{II}(bimH)_2]_n$ (3). Procedure a. A deoxygenated glycerol/ water (1:1) solution (40 mL) of $Fe^{II}(bimH_2)_2(HCOO)_2$[3] ($9.66 \times 10^{-4}$ mol) was slowly added to a stirred solution of 5.8×10^{-3} mol of sodium carbonate in 40 mL of an oxygen-free glycerol/water (1:1) mixture. The resulting reaction mixture was stirred for 48 h under a purified nitrogen atmosphere, during which the resulting complex slowly precipitated as a microcrystalline yellow-green solid. The complex was filtered off, washed with methanol and dried under vacuum. Yield: 63%. Anal. Calcd for $FeC_{12}H_{10}N_8$: C, 44.70; H, 3.11; N, 34.80; Fe, 17.35. Found: C, 44.88; H, 3.15; N, 33.98; Fe, 16.85.

Procedure b. $Fe(CH_3CO_2)_2{\cdot}2H_2O$ (5.8×10^{-4} mol) dissolved in 10 mL of deoxygenated methanol was slowly added to the stirred oxygen-free suspension resulting from mixing 1.17×10^{-3} mol of sodium dissolved in 20 mL of methanol and 1.17×10^{-3} mol of $bimH_2$ suspended in 30 mL of methanol in an inert-atmosphere box, affording a progressive solubilization of the ligand. The microcrystalline yellow-green compound **3** precipitated out of the reaction mixture within 14 h and was filtered off, washed with methanol, and dried under vacuum. Yield: 84%. The resulting dried microcrystalline compound is more sensitive to dioxygen than **2**.

Yellow single crystals of **3** suitable for X-ray diffraction studies were obtained by slow interdiffusion (1 month) between a deoxygenated methanolic solution (45 mL) of $Fe^{II}(CH_3CO_2)_2{\cdot}2H_2O$ (10^{-4} mol) and a deoxygenated methanolic solution (45 mL) of $bimH_2$ (2×10^{-4} mol) deprotonated as indicated above (procedure b).

$\{Fe^{II}(bim)\}_n{\cdot}CH_3OH{\cdot}0.5H_2O$ (4). Compound **4** was obtained in a way similar to method b described for complex **3**, except for the use of a 1:1 molar ratio of deprotonated ligand and ferrous salt. The ligand/ CH_3ONa mixture (1:2 ratio) was stirred for 48 h prior to reaction with the ferrous salt in order to achieve complete deprotonation of the $bimH_2$ ligand. The resulting complex (pale-green powder) was washed with methanol and dried under vacuum. Yield: 95%. Anal. Calcd for $FeC_6H_4N_4.CH_3OH.\ 0.5H_2O$: C, 36.70; H, 3.93; N, 24.47; Fe, 24.40. Found: C, 36.11; H, 3.60; N, 24.33; Fe, 24.25. The resulting pale-green powder is very sensitive to dioxygen, turning to dark green-brown within seconds in the air.

Physical Mesurements. Elemental analyses were carried out at the Laboratoire de Chimie de Coordination Microanalytical Laboratory in Toulouse for C, H, and N and at the Service Central de Microanalyses du CNRS in Vernaison for Fe.

IR spectra were recorded on a Perkin-Elmer 983 Spectrophotometer coupled with a Perkin-Elmer infrared data station. Samples were run as CsBr pellets prepared under nitrogen in the drybox.

Variable-temperature magnetic susceptibility data were obtained as previously described[30] on powdered samples (prepared in the drybox) with a Faraday-type magnetometer equipped with a continuous-flow Oxford Instruments cryostat or a Quantum Design MPMS SQUID susceptometer. Diamagnetic corrections were applied by using Pascal's constants.

Mössbauer measurements were obtained on a constant-acceleration conventional spectrometer with a 25 mCi source of ^{57}Co (Rh matrix). Isomer shift values (δ) throughout the paper are given with respect to metallic iron at room temperature. The absorber was a sample of 120 mg of microcrystalline powder enclosed in a 2 cm diameter cylindrical plastic sample holder, the size of which had been determined to optimize the absorption. Variable-temperature spectra were obtained in the 300–4.2 K range, by using a MD 306 Oxford cryostat, the thermal scanning being monitored by an Oxford ITC4 servocontrol device (±0.1 K accuracy). A least-squares computer program[31] was used to fit the Mössbauer parameters and determine their standard deviations of statistical origin (given in parentheses).

Collection and Reduction of X-ray Data for 1, 2, and 3. A colorless crystal of $[Fe^{II}(bimH_2)_2(CH_3OH)_2](OAc)_2$ (**1**) ($0.50 \times 0.40 \times 0.30$ mm) was coated with vaseline in an inert-atmosphere box and sealed in a Lindemann glass capillary. A yellow-green crystal of $[Fe^{II}(bimH_2)_3]CO_3$ (**2**) ($0.55 \times 0.50 \times 0.25$ mm) and a yellow crystal of $[Fe^{II}(bimH)_2]_n$ (**3**) ($0.55 \times 0.275 \times 0.275$ mm) were mounted in a similar way. The crystals were then transferred to a CAD4 diffractometer. Lattice parameters of the three compounds were obtained from a least-squares analysis of 25 carefully centered reflections with $12° < \theta < 17°$. Tetragonal cells of **2** and **3** were then refined with constraints ($a = b$, $\alpha = \beta = \gamma = 90°$) using the CELDIM program of the CAD4 software. The data were collected at ambient temperature using the $\omega-2\theta$ scan technique at variable rates. A total of 2563 unique reflections were collected up to 27° for **1** (h, $0 \rightarrow 11$; k, $0 \rightarrow 9$; l, $-22 \rightarrow 22$) in space group $P2_1/n$ ($h0l$, $h + l = 2n$, $0k0$, $k = 2n$, alternative of $P2_1/c$). A total of 2728 reflections were collected for **2** up to 28° (h, $-16 \rightarrow 16$; k, $0 \rightarrow 16$; l, $-18 \rightarrow 18$; $|k| \geq |h|$) of which 2567 were unique ($R_{av} = 0.011$ on I) in space group $I4_1$ ($h + k + l = 2n$, $00l$, $l = 4n$). A total of 3354 reflections were collected for **3** in two shells, one up to 30° (h, $-12 \rightarrow 12$; k, $0 \rightarrow 12$; l, $0 \rightarrow 25$; $|k| \geq |h|$), the other one up to 25° (h, $-10 \rightarrow 10$; k, $0 \rightarrow 10$; l, $-21 \rightarrow -1$; $|k| \geq |h|$), of

(30) Luneau, D.; Savariault, J.-M.; Cassoux, P.; Tuchagues, J.-P. *J. Chem. Soc. Dalton Trans.* **1988**, 1225.

(31) Varret, F. *Proceedings of the International Conference on Mössbauer Effect Applications;* Jaipur, India, 1981; Indian National Science Academy: New Delhi, 1982.

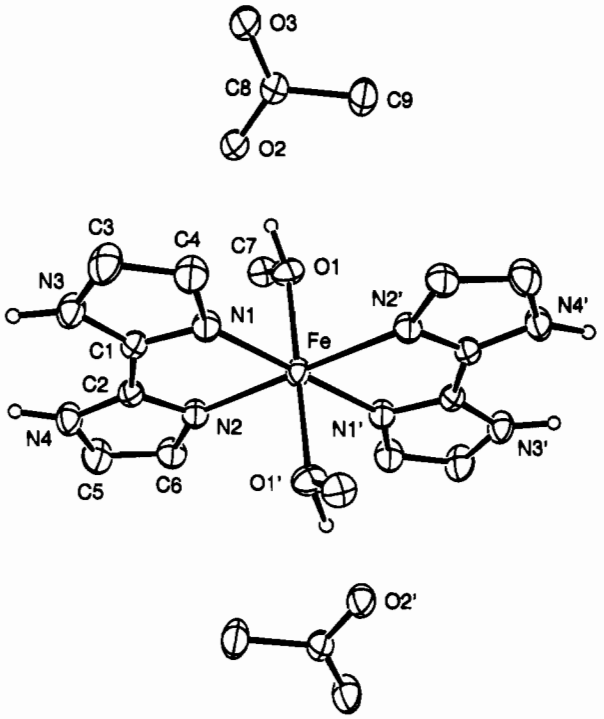

Figure 2. ORTEP view of the $[Fe^{II}(bimH_2)_2(CH_3OH)_2](OAc)_2$ molecule (**1**).

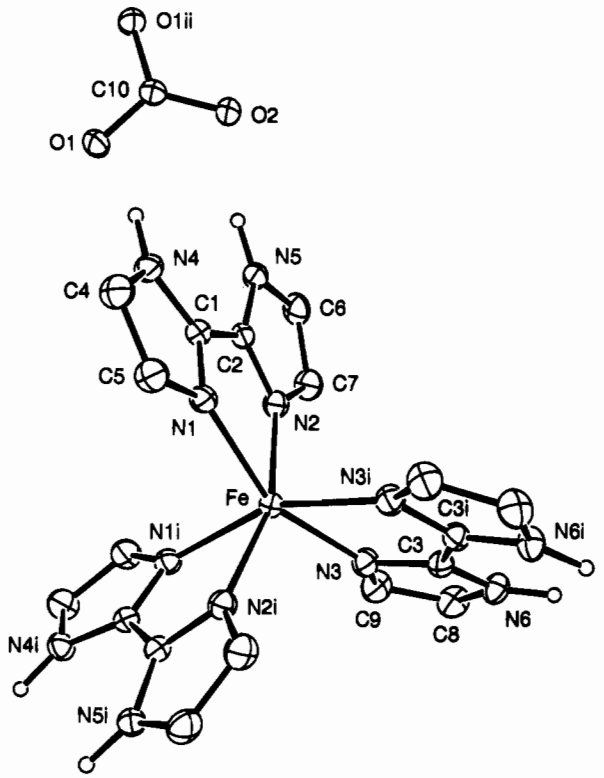

Figure 3. ORTEP view of the $[Fe^{II}(bimH_2)_3]CO_3$ molecule (**2**).

which 3085 were unique (R_{av} = 0.015 on I) in space group $P4_1$ or $P4_3$ ($00l$, $l = 4n$), with the $P4_3$ space group assigned by resolution.

The crystals quality was monitored by scanning three standard reflexions every 2 h. No significant variation was observed during the data collection. The data were corrected for absorption, Lorentz and polarization effects using the MolEN package.[32] Empirical absorption corrections[33] were applied using ψ scan data.

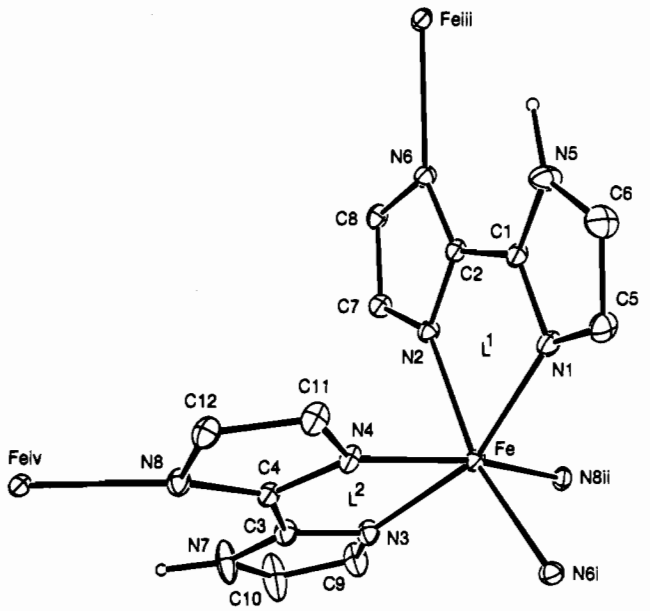

Figure 4. ORTEP view of the $[Fe^{II}(bimH)_2]_n$ molecule (**3**).

Table 1. Crystallographic Data for Complexes **1** , **2** and **3**

	1	**2**	**3**
chem formula	$FeC_{18}H_{26}N_8O_6$	$FeC_{19}H_{18}N_{12}O_3$	$FeC_{12}H_{10}N_8$
	506.3	518.3	322.1
temp (°C)	21	21	21
space group	$P2_1/n$ (No.14)	$I4_1$ (No.80)	$P4_3$ (No.78)
a (Å)	9.021(1)	12.219(1)	8.5144(7)
b (Å)	7.413(1)	12.219(1)	8.5144(7)
c (Å)	17.700(2)	14.334(2)	18.273(3)
β (deg)	97.23(1)		
V (Å^3)	1174.2(4)	2140.1(4)	1324.7(2)
Z	2	4	4
λ(Mo Kα) (Å)	0.710 73	0.710 73	0.710 73
ϱ_{calc} (g cm^{-3})	1.432	1.608	1.615
μ (cm^{-1})	6.9	7.5	11.4
R^a	0.024	0.022	0.032
$R_w{}^b$	0.024	0.023	0.039

[a] $R = (\sum||F_o| - |F_c||)/(\sum|F_o|)$. [b] $R_w = ([\sum w(|F_o|-|F_c|)^2/(\sum w|F_o|)^2]^{1/2})$.

Structure Solution and Refinement. The structures were solved by direct methods with SHELXS 86[34] and refined with SHELX 76[35] programs. The atomic scattering factors, including anomalous dispersion, were taken from standard compilation.[36] All non-hydrogen atoms were refined anisotropically. Hydrogen atoms were placed in idealized generated positions with general refined isotropic thermal parameters, except H(O1) in **1**, which was allowed to vary. The structure of complex **1** was solved in $P2_1/n$. Final R values were R = 0.024 and R_w = 0.024 with unit weights, 1725 reflections ($F_o > 6\sigma(F_o)$), and 158 variable parameters, $\Delta/\sigma_{max} = 0.001$. The $[Fe^{II}(bimH_2)_2(CH_3OH)_2](OAc)_2$ complex molecule **1** is shown in Figure 2 with atom numbering. The structure of compound **2** was solved in the space group $I4_1$, R = 0.022 and R_w = 0.023 with unit weights, 2292 reflections ($F_o > 6\sigma(F_o)$), and 161 variable parameters, $\Delta/\sigma_{max} = 0.001$. Flack[37] value, −0.01(1) confirmed the good enantiomorph. The $[Fe^{II}(bimH_2)_3]CO_3$ complex molecule **2** is shown in Figure 3 with atom numbering. The structure of compound **3** was solved in the space group $P4_3$: Flack value = −0.02(2) instead of 0.89(2) in $P4_1$. Final R values for **3** were R = 0.032 and R_w = 0.039 with $w = 0.85/(\sigma^2(F_o) + 0.0006\,F_o^2)$, 2592 reflections ($F_o > 6\sigma(F_o)$), and 191 variable parameters, $\Delta/\sigma_{max} = 0.002$.

(32) Fair, C. K. *MolEN, Molecular Structure Solution Procedures*, Enraf-Nonius: Delft, The Netherlands, 1990.
(33) North, A. C. T.; Phillips, D. C.; Mathews, F. S. *Acta. Crystallogr., Sect. A: Found. Crystallogr.* **1968**, *A24*, 351.
(34) Sheldrick, G. M. *SHELXS 86. Program for Crystal Structure Solution* ; University of Göttingen: Göttingen, Germany, 1986.
(35) Sheldrick, G. M. *SHELX76. Programm. for Crystal Structure Determination;* University of Cambridge: Cambridge, England, 1976.
(36) *International Tables for X-ray Crystallography* ; Kynoch Press: Birmingham, England, **1974**; Vol. IV.
(37) Flack, H. D. *Acta. Crystallogr., Sect. A* **1983**, *A39*, 876.

Table 2. Selected Interatomic Distances (Å) and Angles (deg) for $[Fe^{II}(bimH_2)_2(CH_3OH)_2](OAc)_2$ (**1**)[a]

Iron Environment			
Fe−O(1)	2.131(2)	Fe−N(1)	2.187(2)
Fe−N(2)	2.174(1)	Fe···Fe(i) = Fe···Fe(ii)	7.413
N(1)−Fe−N(2)	78.59(5)	N(1)−Fe−O(1)	89.13(5)
N(1)−Fe−N(2)′	101.41(5)	N(1)−Fe−O(1)′	90.87(5)
N(2)−Fe−O(1)	89.77(5)	N(2)−Fe−O(1)′	90.23(5)
Biimidazole Ligands			
N(1)−C(1)	1.328(2)	C(1)−N(3)	1.339(2)
N(2)−C(2)	1.324(2)	C(2)−N(4)	1.342(2)
C(3)−N(3)	1.370(3)	C(3)−C(4)	1.351(3)
N(4)−C(5)	1.367(3)	C(4)−N(1)	1.371(3)
C(6)−N(2)	1.370(2)		
Fe−N(1)−C(1)	110.6(1)	Fe−N(2)−C(2)	111.1(1)
Fe−N(1)−C(4)	143.5(1)	Fe−N(2)−C(6)	143.4(1)
Methanol			
Fe−O(1)−C(7)	125.0(1)	Fe−O(1)−H(O(1))	116(1)
Hydrogen bonds			
O(1)···O(2)	2.581(2)	H(O(1))···O(2)	1.62(2)
N(3)···O(2)″	2.705(2)	H(N(3))···O(2)″	1.74
N(4)···O(3)″	2.679(2)	H(N(4))···O(3)″	1.73
O(1)−H(O(1))···O(2)	172	N(3)−H(N(3))···O(2)″	172
N(4)−H(N(4))···O(3)″	167		

[a] Symmetries : single prime, $1-x, 1-y, 1-z$; double prime, $-x, 1-y, 1-z$; i, $x, 1+y, z$; ii, $x, -1+y, z$.

Table 3. Selected Interatomic Distances (Å) and Angles (deg) for $[Fe^{II}(bimH_2)_3]CO_3$ (**2**)[a]

Iron Environment			
Fe−N(1)	2.174(2)	Fe−N(3)	2.221(2)
Fe−N(2)	2.272(2)	Fe···Fe(iv)	7.0829
N(1)−Fe−N(2)	76.30(5)	N(2)−Fe−N(3)	84.72(5)
N(1)−Fe−N(3)	156.26(5)	N(2)−Fe−N(2i)	162.66(7)
N(1)−Fe−N(1i)	98.37(8)	N(2)−Fe−N(3i)	109.22(5)
N(1)−Fe−N(2i)	92.28(5)	N(3)−Fe−N(3i)	76.25(8)
N(1)−Fe−N(3i)	96.48(5)		
Biimidazole Ligands			
N(1)−C(1)	1.327(2)	N(3)−C(3)	1.329(2)
N(1)−(5)	1.372(3)	C(3)−N(6)	1.340(2)
C(1)−N(4)	1.337(2)	C(7)−N(2)	1.378(3)
N(4)−C(4)	1.371(3)	N(5)−C(6)	1.371(3)
N(2)−C(2)	1.321(2)	N(6)−C(8)	1.366(3)
C(2)−N(5)	1.340(2)	C(9)−N(3)	1.375(3)
Fe−N(1)−C(1)	113.6(1)	Fe−N(3)−C(3)	112.4(1)
Fe−N(1)−C(5)	141.3(1)	Fe−N(3)−C(9)	142.4(1)
Fe−N(2)−C(2)	110.7(1)	Fe−N(2)−C(7)	144.0(1)
Carbonate			
C(10)−O(1)	1.292(2)	C(10)−O(2)	1.264(4)
C(10)−O(1ii)	1.292(2)		
O(1)−C(10)−O(2)	120.1(2)	O(1)−C(10)−O(1ii)	119.8(3)
O(2)−C(10)−O(1ii)	120.1(2)		
Hydrogen Bonds			
N(4)···O(1)	2.737(2)	H(N4)···O(1)	1.80
N(5)···O(2)	2.776(2)	H(N5)···O(2)	1.84
N(6)···O(1iii)	2.649(2)	H(N6)···O(1iii)	1.69
N(4)−H(N4)···O(1)	163	N(5)−H(N5)···O(2)	160
N(6)−H(N6)···O(1iii)	169		

[a] Symmetries: i, $1-x, 1-y, z$; ii, $-x, 1-y, z$; iii, $y, 1/2-x, -3/4+z$; iv, $1-y, 1/2+x, 1/4+z$.

In the last refinement cycles an empirical isotropic extinction parameter was refined to 0.85×10^{-7}. The $[Fe^{II}(bimH)_2]$ complex molecule **3** is shown in Figure 4 with atom numbering.

Final difference Fourier maps were featurless for the three compounds. Crystal data are given in Table 1. Selected bond distances and angles for **1**−**3** are presented in Tables 2−4, respectively. All calculations were performed on a MicroVAX 3400 computer. Crystallographic drawings were made by using the ORTEP program.[38] Complete crystallographic data are given in the Supporting Information for all three complexes.[39]

Table 4. Selected Interatomic Distances (Å) and Angles (deg) for $[Fe^{II}(bimH)_2]_n$ (**3**)[a]

Iron Environment			
Fe−N(1)	2.204(2)	Fe−N(3)	2.174(2)
Fe−N(2)	2.208(2)	Fe−N(4)	2.202(2)
Fe−N(6i)	2.190(2)	Fe−N(8ii)	2.210(2)
Fe···Fe(i)	6.2521(3)	Fe···Fe(ii)	6.2441(3)
Fe···Fe(iii)	6.2521(3)	Fe···Fe(iv)	6.2441(3)
N(1)−Fe−N(2)	75.84(8)	N(2)−Fe−N(8ii)	88.94(8)
N(1)−Fe−N(3)	158.79(8)	N(3)−Fe−N(4)	75.93(8)
N(1)−Fe−N(4)	88.57(8)	N(3)−Fe−N(6i)	105.57(8)
N(1)−Fe−N(6i)	88.64(8)	N(3)−Fe−N(8ii)	90.53(8)
N(1)−Fe−N(8ii)	104.53(8)	N(4)−Fe−N(6i)	90.32(8)
N(2)−Fe−N(3)	89.84(8)	N(4)−Fe−N(8ii)	166.46(8)
N(2)−Fe−N(4)	91.02(8)	N(6i)−Fe−N(8ii)	93.36(8)
N(2)−Fe−N(6i)	164.38(8)		
Hydrogen bonds			
N(5)···N(1iii)	3.105(4)	H(N5)···N(1iii)	2.50
N(5)···N(8v)	3.058(4)	H(N5)···N(8v)	2.35
N(7)···N(6vi)	3.063(4)	H(N7)···N(6vi)	2.22
N(5)−H(N5)···N(1iii)	121	N(5)−H(N5)···N(8v)	129
N(7)−H(N7)···N(6vi)	145		

[a] Symmetries: i, $y, -x, 1/4+z$; ii, $y, 1-x, 1/4+z$; iii, $-y, x, -1/4+z$; iv, $1-y, x, -1/4+z$; $v = -1+x, y, z$; vi, $1+x, y, z$.

Results and Discussion

Synthesis and Compositional Studies. We have previously shown[3] that while the reaction of ferrous perchlorate with $bimH_2$ yields tris-chelates regardless of the metal to ligand stoichiometry, bis-chelates or tris-chelates can be obtained according to the metal to ligand ratio when the metal salt includes coordinating anions such as chloride, acetate or formate. However, none of the ferrous bis-chelates of $bimH_2$ previously isolated has been structurally characterized. During the course of our investigations on these ferrous bis-chelates, we noticed that while reactions carried out with warm solutions led to rapid precipitation of the unsolvated species $Fe(bimH_2)_2(CH_3CO_2)_2$,[3] reactions carried out with cold solutions led to slow precipitation of a solvated species (**1**) includind two molecules of methanol. The methanol content being exactly the same for the numerous reactions performed, we have recrystallized this new species in view of the interest of the four imidazole nitrogen and two oxygen ligand environment required for the ferrous iron of such species.

Synthesis of complex **2** resulted from the study of competition reactions between the formate anions of $Fe^{II}(bimH_2)_2(HCOO)_2$[3] and HCO_3^- anions brought by addition of sodium bicarbonate to methanolic solutions of the bis-chelate precursor. Our initial goal was to evaluate the ability of such anions to displace the formate anions as shown for the non-heme iron(II) of PS 2 and to model the suspected four imidazole and one bicarbonate coordination sphere of this natural ferrous site.[7b,e] As shown by elemental analyses and Mössbauer spectroscopy, the precipitates afforded by these reactions are mixtures of **2** and $Fe^{II}(bimH_2)CO_3 \cdot x$MeOH. Variations in the reaction time and/or sodium bicarbonate concentration modified the ratio of the two components of the mixture, although complex **2** remained always the major component. These observations led us to suspect the initial formation of a quite unstable iron/$bimH_2$ bis-chelate which subsequently affords **2** (the most stable species)

(38) Johnson, C. K. ORTEP. Report ORNL-3794; Oak Ridge National Laboratory: Oak Ridge, TN 1965.
(39) Supporting Information.

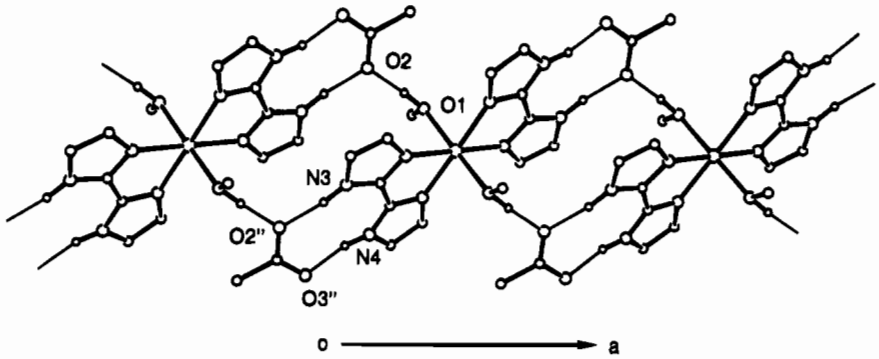

Figure 5. Projection of three $[Fe^{II}(bimH_2)_2(CH_3OH)_2](OAc)_2$ molecules (**1**) showing the hydrogen bond network (thin lines).

and $Fe^{II}(bimH_2)CO_3 \cdot xMeOH$ (soluble species) through the following redistribution reaction:

$$2\ Fe^{II}(bimH_2)_2CO_3 \rightarrow Fe^{II}(bimH_2)_3CO_3 + Fe^{II}(bimH_2)CO_3$$

Understandably, we were unable to isolate pure samples of the ferrous mono-chelate of $bimH_2$. However, with long enough reaction times (at least three weeks) and ratios of sodium bicarbonate close to stoichiometry or higher we were able to isolate pure samples of **2**. The same ferrous tris-chelate of $bimH_2$ (**2**) was also obtained through reaction of sodium bicarbonate with a mixture of ferrous perchlorate and $bimH_2$ regardless of the iron/$bimH_2$ and CO_3HNa/ precursor complex ratios.

It is worth to notice that regardless of the synthetic route, the metatheses with HCO_3^- afford ferrous compounds including always CO_3^{2-}. This result is in line with previous studies carried out with Co(III)[10] and Fe(III)[11a] complexes and CO_3HNa. Similarly, CO_3^{2-} is the most probable synergistic anion of transferrins, the only structurally characterized metalloprotein including a carbon dioxide related bidentate ligand.[40,12ab]

Synthesis of complex **3**, $[Fe^{II}(bimH)_2]_n$, resulted initially from the study of competition reactions between the formate anions of $Fe^{II}(bimH_2)_2(HCOO)_2$[3] and carbonate anions brought by addition of CO_3Na_2 to methanolic solutions of the bis-chelate precursor. These experiments showing that the basicity of the reaction medium was high enough to induce deprotonation of $bimH_2$, we confirmed the synthesis of the unprecedented ferrous bis-chelate of the $bimH^-$ biimidazolate monoanion through direct reaction between a ferrous salt and the deprotonated ligand in methanol. $[Fe^{II}(bimH)_2]_n$ (**3**) affords the first example of bridging biimidazolate monoanion. It corresponds to the non-previously described coordination mode (C) depicted in Figure 1.

As complex **3** was the only product obtained for MeONa/ $bimH_2$ ratios between 1 and 3 in the later synthetic route, we were led to conclude that the bis-chelate nature of **3** is under control of the Fe:L ratio. This observation allowed us to show that a 1:1 or lower L:Fe ratio associated with a MeONa/$bimH_2$ ratio higher than 2 affords the novel ferrous mono-chelate of the biimidazolate bim^{2-} dianion, $\{Fe^{II}(bim)\}_n$ (**4**), as the only product of the reaction between a ferrous salt and the deprotonated ligand in methanol.

Molecular Structure of 1, 2, and 3. Complex 1. The structure consists of $[Fe^{II}(bimH_2)_2(CH_3OH)_2]^{2+}$ complex cations and acetate anions (Figure 2). The iron, situated on a crystallographic inversion center in the unit cell, is coordinated to the N(1) and N(2) nitrogen atoms of two $bimH_2$ ligands trans to each other and O(1) oxygen atom of two methanol molecules which are also trans to each other. The main distorsion of the resulting octahedral coordination sphere originates in the small N(1)···N(2) bite of the chelating ligand (N(1)−Fe−N(2) = 78°6) (Table 2). The resulting rectangular distortion of the N(1), N(2),N(1)′,N(2)′ plane and departure of the faces of the coordination octahedron from equilaterality,[39] affords elongations along two pseudo-C_3 axis perpandicular to the {N(1)O(1)N(2) and N(1)′O(1)′N(2)′} and {N(1)′O(1)N(2)′ and N(1)O(1)′N(2)} faces of the coordination octahedron, respectively. Furthermore, the Fe−O(1) distance (2.131(2) Å) is shorter than the Fe−N(1) (2.174(1) Å) and Fe−N(2) (2.187(2) Å) ones, and as a result of all three distortions the coordination sphere may be described as a N(1)N(2)N(1)′N(2)′ based octahedron significantly compressed along the O(1)···O(1)′ C_2 axis.

The $[Fe^{II}(bimH_2)_2(CH_3OH)_2]^{2+}$ complex cations are linked together into infinite chains along *a* through O(1)−H(O1)···O(2), N(3)−H(N3)···O(2)″ and N(4)−H(N4)···O(3)″ hydrogen bonds involving the amine nitrogen atoms of all $bimH_2$ ligands, all coordinated methanol molecules, and noncoordinated acetate anions (Figure 5). These chains are stacked along *b* with an intermetallic inter-chain distance of 7.413 Å, while the shortest intermetallic intrachain distance is 9.021 Å.

Complex 2. The structure consists of $[Fe^{II}(bimH_2)_3]^{2+}$ complex cations hydrogen bonded to carbonate dianions (Figure 3). The coordination geometry of the iron(II) center can be described as a distorted octahedron including six nitrogen atoms originating from three chelating $bimH_2$ ligands. As in complex **1**, the main distortion results from the small N−Fe−N bite angle (76°3) imposed by the $bimH_2$ ligand and the resulting range of iron-nitrogen distances (Table 3). The Fe−N(2) distance (2.272(2)Å) being larger than the Fe−N(1) (2.174(2)Å) and Fe−N(3) (2.221(2)Å) ones, the coordination octahedron is slightly elongated along N(2)−N(2i) (pseudo-C_2 axis). For the same reason, the coordination octahedron is compressed along a pseudo-C_3 crystallographic axis perpendicular to the N(1), N(2i), N(3i) and N(1i), N(2), N(3) faces[39] as a result of the trapezoidal arrangement of the N(1), N(1i), N(3), and N(3i) equatorial donors. A similarly distorted coordination octahedron has been previously evidenced for the related $[Fe^{II}(bbzimH_2)_3]^{2+}$ complex cation in $[Fe^{II}(bbzimH_2)_3](ClO_4)_2$ ($bbzimH_2$ = 2,2′-bibenzimidazole).[3]

Each $[Fe^{II}(bimH_2)_3]^{2+}$ complex cation is connected to three carbonate dianions through six strong N−H···O hydrogen bonds with 2.649(2)−2.776(2) Å N···O distances, and reciprocally each carbonate dianion is connected to three complex cations through six hydrogen bonds (Figure 6). The crystal packing afforded by this highly symmetrical and dense 3D network of hydrogen bonds results in a 7.083 Å intermetallic distance between adjacent complex cations. The three C−O distances of the carbonate dianion, although not rigorously equal (1.264(4)−1.292(2) Å) are intermediate between those usually ob-

(40) Anderson, B. F.; Baker, H. M.; Norris, G. E.; Rice, D. W.; Baker, E. N. *J. Mol. Biol.* **1989**, *209*, 711.

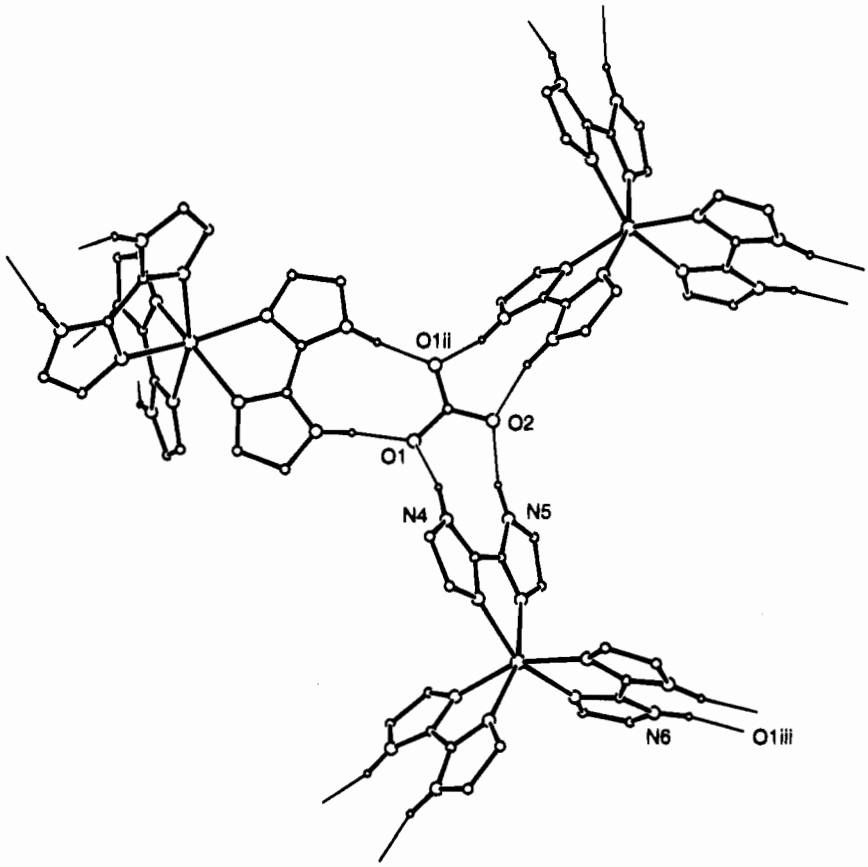

Figure 6. Projection of five $[Fe^{II}(bimH_2)_3]CO_3$ molecules (**2**) showing the hydrogen bond network (thin lines).

served for single and double C−O bonds,[10a,41] indicating important delocalization effects.[42]

Complex 3. The ferrous center of each $[Fe^{II}(bimH)_2]$ neutral unit is chelated to two biimidazolate monoanions cis to each other, through N(1) and N(2) (L^1) and N(3) and N(4) (L^2) (Figure 4). Two deprotonated amine nitrogen donors (N(6i) and N(8ii)) arising respectively from the L^1i and L^2ii biimidazolate ligands of adjacent complex molecules supplement the iron(II) coordination octahedron. At variance with the iron ligand environment in complex **2**, the six Fe−N distances (2.174(2) to 2.210(2) Å) are close to each other (Table 4) affording a ligand environment similar to that evidenced in the case of the $[Fe^{II}(bbzimH_2)_3]^{2+}$ complex cation of $[Fe^{II}(bbzimH_2)_3](Cl)_2$.[3] The small N−Fe−N bite angles (~76°) imposed by the L^1 and L^2 chelating ligands associated with the constraints resulting from the bridging of the iron atom to four nearest neighbors through imidazolate moieties pertaining to four biimidazolate ligands afford important distortions of the coordination octahedron. This is clearly reflected by the distances and angles between atoms defining the faces of the coordination octahedron and dihedral angles between opposite faces[39] which do not allow to distinguish any satisfactory symmetry axis, at variance with the case of complex **2**.

Each biimidazolate monoanion is simultaneously coordinated to one iron atom in a bidentate mode through the imine nitrogen atoms of both imidazole rings and in a monodentate mode to another iron atom through the deprotonated amine nitrogen atom of its imidazolate ring. Consequently, all iron atoms situated at the same z value are bridged through the imidazolate rings of $bimH^-$ ligands affording a sheet spanning *a,b*.[39] These sheets are linked together through similar imidazolate bridges along the [001] perpendicular direction[39] affording a 3D network in which each $[Fe^{II}(bimH)_2]$ molecule is linked to four nearest neighbors through N−C−N bridges. The resulting intermetallic separation is 6.2441(3) Å for the iron atoms related through the $1 - y, x, -1/4 + z$ and $y, 1 - x, 1/4 + z$ symmetry operators and 6.2521(3) Å for the iron atoms related through the $-y, x, -1/4 + z$ and $y, -x, 1/4 + z$ symmetry operators.

The crystal packing afforded by this 3D network of $[Fe^{II}(bimH)_2]$ molecules is supplemented by an hydrogen bond lattice involving the N(5)−H(N5) (L^1) and N(7)−H(N7) (L^2) groups and the N(6) and N(8) (or N(1)) deprotonated amine (or imine) nitrogen atoms of adjacent molecules (Figure 7 and Table 5).

IR Spectroscopy. Table 6 lists some pertinent IR frequencies for the isolated $bimH_2$ ligand and complexes **1**−**4** together with our proposed assignments. In agreement with reports on complexes including the same or similar ligands,[3,43] the overall appearance of the spectra of complexes **1** and **2** is similar to that of the isolated ligand and include the following general features: (i) NH + CH stretches spreading out from ca. 3250 to 2400 cm^{-1}, (ii) N−H in plane bending frequencies nearby 1550 and 1150 cm^{-1}, (iii) imidazole ring stretching absorptions in the 1460−1370 cm^{-1} range and characteristic Δ' ring beating in the 1333−1315 cm^{-1} region, (iv) C−H in-plane bending frequencies in the 950−900 cm^{-1} range, (v) two to three in-plane imidazole ring bending absorptions (780−730 cm^{-1}) and two imidazole ring torsion absorptions (700−610 cm^{-1} range).

With the exception of the N−H frequencies which are modified in the case of **3** and completely lacking for **4** (Table 6), the same comments hold for complexes **3** and **4**. As evidenced by the absence of N−H stretching and bending

(41) Churchill, M. R.; Lashewycz, R. A.; Koshy, K.; Dasgupta, T. P. *Inorg. Chem.* **1981**, *20*, 376.

(42) (a) Churchill, M. R.; Davies, G.; El-Sayed, M. A.; El-Shazly, M. F.; Hutchinson, J. P.; Rupich, M. W.; Watkins, K. O. *Inorg. Chem.* **1979**, *18*, 2296. (b) Churchill, M. R.; Davies, G.; El-Sayed, M. A.; El-Shazly, M. F.; Hutchinson, J. P.; Rupich, M. W. *Inorg. Chem.* **1980**, *19*, 201.

(43) Lane, T. J.; Nakagawa, I.; Walter, J. L.; Kandathil, J. *Inorg. Chem.* **1962**, *1*, 267.

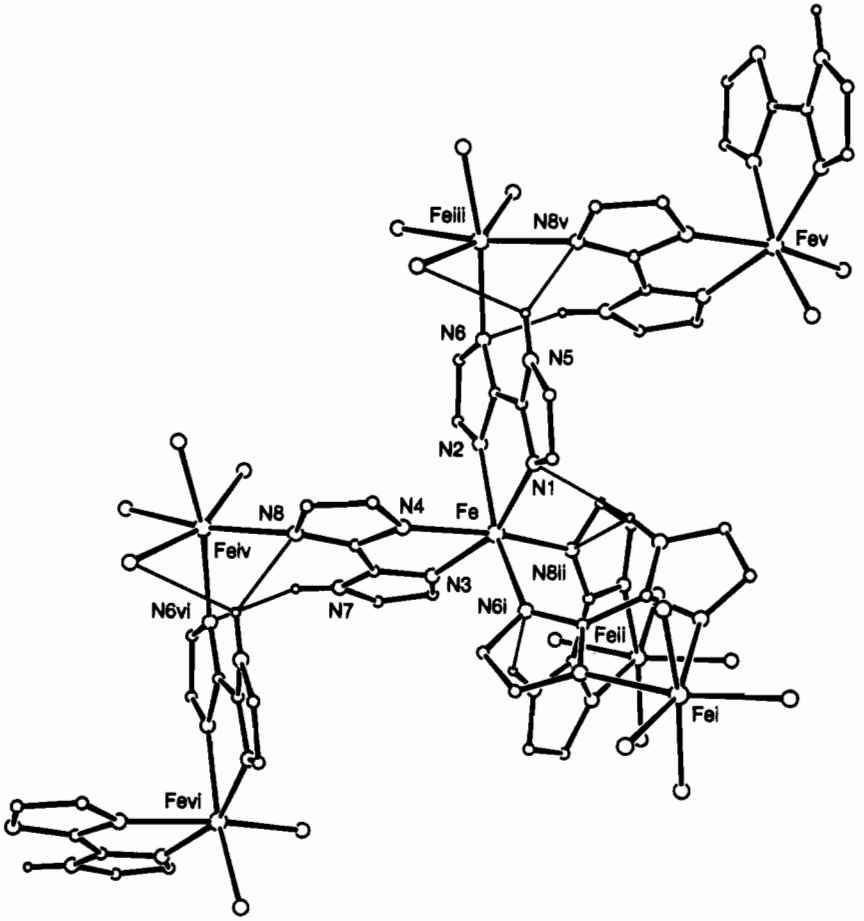

Figure 7. Projection of seven $[Fe^{II}(bimH)_2]_n$ molecules (**3**) showing the hydrogen bond network (thin lines).

Table 5. Selected Infrared Data (cm^{-1}) for $bimH_2$ and Complexes **1**–**4**

	$bimH_2$	**1**	**2**	**3**	**4**
ν_{NH} (stretching)				3355	
$\nu_{NH} + \nu_{CH}$ (stretching)	3173–2544	3250–2500	3142–2400		
ν_{CH} (stretching)				3157–2560	3120–2480
ν_{N-H} (in-plane bending)	1580 sh, 1543	1540	1532	1586	
imidazole ring stretching	1433, 1403	1455–1390	1460–1370	1449, 1404	1498–1410
Δ' imidazole ring beating	1333	1327	1322	1315	1328
ν_{N-H} (in-plane bending)	1144	1178	1179	1145 sh	
ν_{C-H} (imidazole ring bending)	1118, 1104	1120	1121	1127, 1104, 1083	1134–1098
ν_{C-H} (in-plane bending)	939, 915	923	984, 911	944, 912	950, 900
ν_{N-H} (out of plane bending)	887, 829	889	887	863, 845	
imidazole ring Δ in-plane bending	763, 748, 736	775, 754, 736	780, 766	773, 755, 732	770, 760, 732
Γ imidazole ring torsion	689, 616	697, 660	693, 622	702	700
ν_{Fe-L}		470, 426, 354, 300, 278	494, 426, 250	594, 507, 429, 250	515, 485, 438, 410, 290
ν_{OH}		3400 (MeOH)	3420 (MeOH)		3607 (H_2O) 3389 (MeOH)
ν_{C-O} (stretching, MeOH)		1025	1035 sh		1032
ν_{COO^-} (asym)		1561			
ν_{COO^-} (sym)		1407			
ν_3 (CO_3)			1532, 1507, 1397		
ν_1 (CO_3)			1090, 1060		
ν_2 (CO_3)			860, 850		
ν_4 (CO_3)			780–766		

absorptions, the biimidazolate ligand is coordinated to the metal center of compound **4** in its fully deprotonated form. This is confirmed by the 1:1 M/L stoechiometry and the lack of absorptions corresponding to counterions. In the 4000–2000 cm^{-1} range, one strong and several weaker absorptions (3355 and 3157–2560 cm^{-1} range, respectively) are observed for single crystals or powder samples of complex **3**. On the basis of the exclusive presence of biimidazole monoanions in the structure of **3** (single-crystal X-ray diffraction and elemental analyses) we conclude that the bridging bimH monoanion exhibits separated NH and CH imidazole stretching modes. Confirmation of this interpretation arises from the lack of absorption at (or around) 3355 cm^{-1} in the IR spectra of complex **4** in which the characteristic CH imidazole stretching modes (3120–2480 cm^{-1}) are very similar to those of **3**. Thus, the NH and CH imidazole stretching modes may be regarded as a fingerprint of the protonation state of coordinated biimidazole ligands: while they are overlapping in the 3250–2400 cm^{-1} range for $bimH_2$, they are well separated for the $bimH^-$ monoanion and the 3355 cm^{-1} NH stretching mode is lacking

Table 6. Representative Least-Squares Fitted Mössbauer Data for Complexes **1**−**4**[a,b]

		1	2	3	4
293 K	δ	1.071(2)	1.041(2)	1.039(1)	0.965(2)
	ΔE_Q	3.668(2)	0.796(2)	1.878(1)	2.494(2)
	$\Gamma/2$	0.163(4)	0.170(3)	0.155(1)	0.240(3)
80 K	δ	1.196(1)	1.183(2)	1.146(2)	1.021(1)
	ΔE_Q	3.706(1)	1.695(2)	2.426(2)	2.982(1)
	$\Gamma/2$	0.167(2)	0.192(3)	0.188(2)	0.243(2)
4.3 K	δ	1.226(1)	1.200(1)	1.143(2)	1.037(7)
	ΔE_Q	3.707(1)	1.870(1)	2.402(3)	3.20(2)
	$\Gamma/2$	0.174(2)	0.190(2)	0.202(2)	0.25(2)

[a] δ = isomer shift (mm s^{-1}), ΔE_Q = quadrupole splitting (mm s^{-1}), $\Gamma/2$ = half-width of the lines. [b] Statistical standard deviations are given in parentheses.

for the bim^{2-} dianion. This remark is important in view of the lack of information concerning the IR spectra of complexes including biimidazolate mono- or dianions.[22a,26]

Involvement of the biimidazole imine nitrogen atoms in the coordination to the metal center in a bidentate mode is not only evidenced by the crystal molecular structure of **1**−**3** but also by the significant shifts of the imidazole in-plane ring bending and ring torsion absorptions in complexes **1**−**4**, compared to the isolated ligand. This observation is in agreement with restriction of in-plane ring bending and torsion resulting from coordination of both imine nitrogen atoms of $bimH_2$. The involvement of the deprotonated amine nitrogen atoms of $bimH^-$ (**3**) and bim^{2-} (**4**) in the coordination to another metal center further shifts these absorptions as a consequence of the additional decrease in ring motions (Table 6).

Owing to the lack of absorptions in the 600−200 cm^{-1} range for uncoordinated $bimH_2$, absorptions occuring in this range for the four complexes may be assumed to result from coordination (Table 6). Among these low-frequency absorptions, the one observed between 290 and 250 cm^{-1} for complexes **1**, **3**, and **4** is probably a N−M−N bending frequency, as suggested by previous IR and Raman spectroscopic studies.[44]

The presence of methanol assumed for complexes **1**, **2**, and **4** on the grounds of the elemental analyses and further confirmed by the crystal molecular structure for **1**, is also evidenced by the characteristic OH and C−O stretching modes nearby 3400 and 1030 cm^{-1}, respectively. The absence of methanol in the crystals of **2** and the higher O−H and C−O stretching frequencies for powders of **2** compared to **1** indicate that MeOH is interstitial in samples of **2** resulting from precipitation. Similar observations can be made for the methanol and water molecules present in complex **4**: while the relatively high ν_{C-O} (MeOH) and ν_{O-H} (water) frequencies indicate that these solvents are not coordinated, the relatively low ν_{O-H} (MeOH) frequency indicates the participation of methanol in hydrogen bonds.

The asymmetric and symmetric absorptions observed for the uncoordinated acetates of **1** (crystal structure) are situated at 1561 and 1407 cm^{-1}, respectively. The Δ (= $\nu_{as}(CO_2^-)$ − $\nu_s(CO_2^-)$) value of 154 cm^{-1} is lower than expected for an ionic acetate (164 cm^{-1}),[45] reflecting a lowered difference in the stretching ability of the C−O$^-$ and C=O bonds probably arising from the involvment of both acetate oxygen atoms in hydrogen bonds ("pseudobridging" arrangement described in the molecular structure section).

Complex **2** exhibits several typical carbonate IR absorptions (Table 6) and the splitting of the main absorption (ν_3, 1397 cm^{-1}) seems to suggest coordination of CO_3^{2-} to the metal center[46] in apparent contradiction with the crystal molecular structure of **2** evidencing that the iron is chelated to three $bimH_2$ ligands. However, each carbonate dianion is connected to three $[Fe^{II}(bimH_2)_3]^{2+}$ complex cations through six strong hydrogen bonds involving symmetrically all three carbonate oxygen atoms. Consequently, the carbonate dianion is in a pseudotridentate symmetrical environment which may afford a ν_3 splitting similar to that observed for several complexes including symmetrical tridentate bridging carbonates.[42a,47]

Table 7. Effective Magnetic Moment (μB) at Selected Temperatures for Complexes **1**−**4**

	μ_{eff}				
complex	T = 300 K	T = 100 K	T = 50 K	T = 20 K	T = 2 K
$[Fe^{II}(bimH_2)_2(CH_3OH)_2](OAc)_2$ (**1**)	5.28	5.24	5.18	5.12	4.23
$[Fe^{II}(bimH_2)_3]CO_3$ (**2**)	5.30	5.23	5.09	4.93	4.06
$[Fe^{II}(biimH)_2]_n$ (**3**)	5.39	5.29	5.20	5.01	4.22
$\{Fe^{II}(biim)\}_n$ (**4**)	5.57	5.26	5.39	13.05	5.46

Mössbauer Spectroscopy. With the exception of the 4.3 K spectrum of **4** discussed at the end of this section, the Mössbauer spectra of complexes **1**−**4** recorded at 293, 80, and 4.3 K consist of a single quadrupole split doublet.[39] They were least-squares fitted with Lorentzian lines and the resulting isomer shift (δ) and quadrupole splitting parameters (ΔE_Q) are listed in Table 6. The δ and ΔE_Q values clearly indicate the presence of high-spin (HS) iron(II) in a distorted octahedral ligand environment for the four complexes. The δ values are weakly temperature dependent due to second order Doppler shift.[48] The isomer shift values for complex **1** and complexes **2**−**4** are comparable to those of other complexes with N_4O_2 and N_6 ligand environments, respectively.[3]

The low temperature ΔE_Q values are relatively large for complexes **1**, **3**, and **4** indicating that the T_{2g} orbital triplet is split by crystal field distortions, affording lower than octahedral symmetry and that the lower state is an orbital singlet. Decrease of ΔE_Q at room temperature indicates the presence of excited T_{2g} levels within thermal reach in complexes **2**−**4**.[49]

The crystal molecular structure of $[Fe^{II}(bimH_2)_2(CH_3OH)_2](OAc)_2$ (**1**) indicates that the distortion of the octahedral geometry is essentially axial and results from a compression along O(1)···O(1)′. Consequently, if O(1)···O(1)′ is taken as the C_4 quantization axis, $|xy\rangle$ should be the orbital singlet ground state.[50] The 3.71 mm s^{-1} ΔE_Q value at 4.3 K is in agreement with a singlet ground state and the 3.67 to 3.71 mm s^{-1} ΔE_Q variation in the 300−80 K temperature range indicates that the energy separation between the singlet ground state and the higher orbital states (subsequently abbreviated D_s) is large enough to prevent thermal population of the higher orbital states at 300 K.

In the case of $[Fe^{II}(bimH_2)_3]CO_3$ (**2**) the crystal structure indicates a rhombic distortion of the octahedral symmetry including an axial compression along a pseudotrigonal axis; consequently, the ground state is probably a doublet split by the rhombic distortion. The 1.87 mm s^{-1} ΔE_Q value at 4.2 K substantiates a doublet ground state, and its strong temperature dependence indicates that the energy separation between the ground state and the first higher orbital state is small enough to

(44) (a) Cordes, M. M.; Walter, J. L. *Spectrochim. Acta* **1968**, *24A*, 1421. (b) Goodgame, B. M. L.; Goodgame, M.; Rayner Canham, G. W. *Inorg. Chim. Acta* **1969**, *3*, 406.
(45) Deacon, G. B.; Phillips, R. J. *Coord. Chem. Rev.* **1980**, *33*, 227.
(46) Gatehouse, B. M.; Livingstone, S. E.; Nyholm, R. S. *J. Chem. Soc.* **1958**, 3137.
(47) (a) Davis A. R.; Einstein, F. W. B.; Curtis, N. F.; Martin, J. W. L. *J. Am. Chem. Soc.* **1978**, *100*, 6258. (b) Harada, H.; Kodera, M.; Vuckovic, G.; Matsumoto, N.; Kida, S. *Inorg. Chem.* **1991**, *30*, 1190.
(48) Greenwood, N. N.; Gibbs, T. C. *Mössbauer Spectroscopy*, Chapman and Hall: New York, 1971; Chapter 6.
(49) Ingalls, R. *Phys. Rev.* **1964**, *133*, A787.
(50) Sams, J. R.; Tsin, T. B. *Inorg. Chem.* **1975**, *14*, 1573.

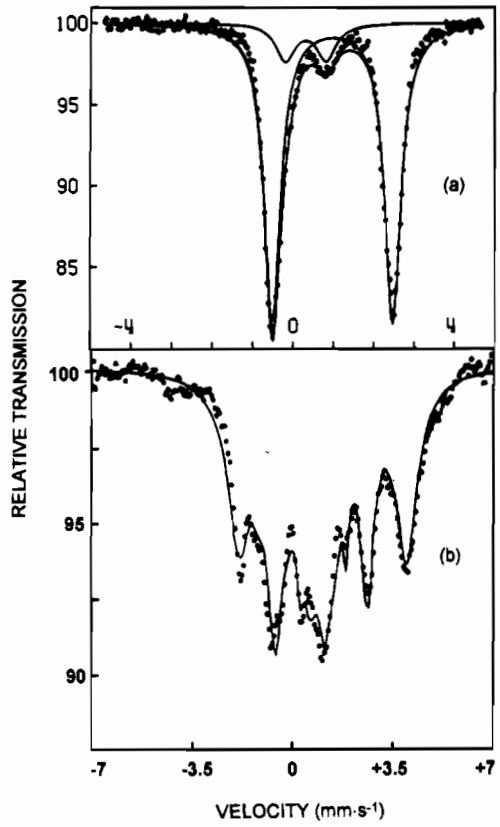

Figure 8. Mössbauer spectra of $\{Fe^{II}(bim)\}_n$ (**4**) at: (a) 80 and (b) 4.2 K.

result in a significant thermal population of the later. For such small orbital level separations, the role of the spin−orbit coupling becomes very important and an understanding of the system would require much more elaborate studies which are beyond the scope of this paper.

The 2.40 mm s^{-1} ΔE_Q value for $[Fe^{II}(bimH)_2]_n$ (**3**), at 4.3 K and its temperature dependence indicate that the energy separation between the ground state and the first higher orbital state is small enough to result in a significant thermal population of the later. The low temperature maximum ΔE_Q value is about 40% lower than the maximum value of 4 mm s^{-1} expected for an isolated singlet ground state.[50] This can be attributed to the effect of the spin−orbit interaction. Actually, an axial splitting ~5 times greater than the spin−orbit constant, λ (− 144 K for the free Fe^{2+} ion[51]), would qualitatively explain both the temperature dependence of ΔE_Q and the reduced low temperature maximum.[49] It is possible to roughly assess this energy separation assuming that the ΔE_Q slope varies as D_s^{-1} in the high-temperature range, as shown in a full vibronic treatment of high-spin Fe(II) ions in a K_2ZnF_4 matrix.[52] The slope $d\Delta E_Q/dT$ can be accurately determined by linear regression as -2.57 10^{-3} mm s^{-1} K^{-1} yielding an energy separation D_s of 903 K. However, due to the very low symmetry of the coordination octahedron it is not possible to assess the exact nature of the ground orbital state in complex **3**.

The Mössbauer spectra of complex **4** result from the presence of two overlapping quadrupole split doublets between 293 and 25 K (Figure 8a). The Mössbauer parameters of the minor doublet (12.5% of the total iron, $\delta = 0.419(10)$, $\Delta E_Q = 1.015(9)$ mm s^{-1} at 80 K) are characteristic of an iron(III) site which probably results from partial dioxygen oxidation of **4** (Experimental Section). Sealing the sample holder with melted paraffine in the drybox prior to its transfer to the spectrometer and flushing carefully the sample chamber with purified nitrogen or helium immediatly after introduction of the sample allowed to reduce this ferric component from an initial value of 29% to the above-mentioned lowest value of 12.5%.

The Mössbauer parameters of the major doublet ($\delta = 1.021(1)$, $\Delta E_Q = 2.982(1)$ mm s^{-1} at 80 K) indicate that the ground state of the HS iron(II) is an orbital singlet. This iron(II) site is magnetically ordered at 4.3 K (Figure 8b). The magnetic spectrum indicates the presence of magnetic and quadrupolar interactions of the same order of magnitude and its analysis requires to compute the exact solutions of the nuclear spin Hamiltonian.[53] The spacings between the six lines of this magnetic spectrum exclude the axial symmetry characterized by $\eta = 0$ and H_i parallel to the principal axis of the electric field gradient (EFG). The best parameters resulting from the least-squares fit of the experimental spectrum are: $\eta = 0.50(2)$, $H_i = 103(2)$ kOe, θ (angle between the EFG z axis and the H_i direction) = 56(5)°, γ (angle between the EFG x axis and the projection of the H_i direction onto the xOy EFG plane) = 90(5)°. These parameters have been obtained by considering different line width for the components of the Zeeman spectrum, which indicates a small but significant distribution of the internal magnetic field. The quite small H_i value is characteristic of well-documented orbital effects.[48] The fit shows unambiguously that the principal EFG component is negative. In addition, the least-squares fit of the 4.3 K experimental spectrum indicates the presence of small residual HS Fe(II) and Fe(III) paramagnetic fractions (Par) coexisting with the Fe(II) and Fe(III) magnetic components (Mag) ($Fe(II)_{Mag} = 75(2)\%$, $Fe(II)_{Par} = 14(1)\%$, $Fe(III)_{Mag} = 8\ (1)\%$, $Fe(III)_{Par} = 3\ (1)\%$). Common values of the δ and ΔE_Q parameters have been assumed for the magnetic and paramagnetic components of the spectrum during the fitting procedure yielding $\delta = 1.037(7)$ and $\Delta E_Q = -3.20(2)$ mm s^{-1} for the Fe(II) components and $\delta = 0.45$(fixed) and $\Delta E_Q = -1.154(7)$ mm s^{-1} for the Fe(III) components.

Magnetic Susceptibility. The molar magnetic moments of powdered samples of complexes **1**−**4** determined in the 300−2 K temperature range are gathered in Table 7. The effective magnetic moment per iron at 300 K is generally higher than the spin only value of 4.9 μ_B for $S = 2$ as usually observed for high-spin iron(II) complexes. The $^5T_2$ ground state is split by the spin orbit coupling giving levels separated by energies on the order of kT (thermally populated in the high-temperature range) which results in slightly temperature dependent magnetic moments above *ca.* 60 K.[54] The relatively small dependence of the magnetic moment of complexes **1**−**3** with temperature indicates that none of these complexes experiences noticeable magnetic exchange interactions. The decrease in their magnetic moment is situated between 25 and 2 K further indicating the presence of zero-field splitting of the high-spin iron(II) ground state. This conclusion agrees well with the results of the X-ray structural determination leading to description of complexes **1** and **2** as isolated mononuclear species in which the iron is surrounded by ligands affording a distorted octahedral coordination sphere and showing that the shortest Fe···Fe distances are 7.41 (**1**) and 7.08 Å (**2**).

The imidazolate bridges between next nearest iron atoms in the 3D network of molecules in complex **3** afford Fe···Fe distances large enough (*ca.* 6.25 Å) to explain the lack of superexchange magnetic interactions. However, in the case of imidazolate- (im^--) bridged copper(II) complexes, several authors have evidenced im^--mediated superexchange interac-

(51) Trees, R. E. *Phys. Rev.* **1951**, *82*, 683.
(52) Ducouret-Cérèze, A.; Varret, F. *J. Phys. (Paris)* **1988**, *49*, 661.
(53) Price, D. C.; Varret, F. *Advances in Mössbauer Spectroscopy;* Thosar, B. V., Iyengar, P. K., Eds.; Elsevier: Amsterdam, 1983; Chapter 6, p 369.
(54) Mabbs, F. E.; Machin, D. J. *Magnetism and Transition Metal Complexes;* Chapman and Hall: London, 1973.

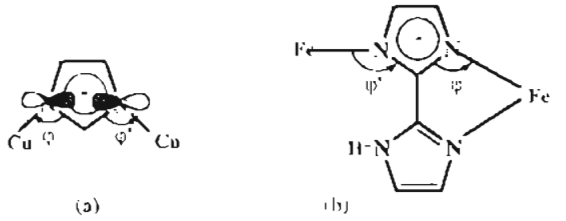

Figure 9. Schematic drawing of (a) the Cu−imidazolate−Cu fragment, (b) the Fe−bimH−Fe fragment in $[Fe^{II}(bimH)_2]_n$ (**3**).

tions ranging from moderately antiferromagnetic to weakly ferromagnetic.[25,55] These interactions can be mediated by σ and π ligand-based orbitals although several authors have shown that superexchange proceeds mainly through the σ orbitals in the case of im^-.[25,55b-d] CNDO/2 calculations indicate that the highest occupied σ orbital of im^- which can provide an interaction pathway for the d_{z^2} orbitals of two Cu(II) ions has major contributions from two nitrogen orbitals oriented as indicated in scheme a of Figure 9.[25] Consequently, an increase of the M−N−C φ and φ' angles improves the overlap between these nitrogen orbitals and the copper $d_{x^2-y^2}$ orbitals, and the overlap should be largest when both Cu−N vectors are parallel to the imidazolate C−C bond.[55c] In agreement with this analysis, Bencini et al.[55d] have shown by extended Hückel calculations on model Cu−im^-−Cu units that the extent of the antiferromagnetic coupling should decrease with φ in the range 180−158°, ferromagnetic coupling should occur for $\varphi \sim 158°$, and again antiferromagnetic coupling should occur for $\varphi < 158°$. In the case of distorted octahedral high-spin iron(II), the situation is much more complex. However, a qualitative analysis shows that φ angles are particularly small (114−115°) while φ' angles are slightly larger (133°) as a result of the coordination of each $bimH^-$ anion in a bidentate mode to one iron and in a monodentate mode to another iron of the 3D network of **3** (Figure 9, scheme b). This situation results in Fe−N···N angles (147−163°) closer to 158 than 180° which may explain why $bimH^-$-mediated superexchange interactions are not noticeable for complex **3**.

The temperature dependence of the magnetic susceptibility of **4** studied in the 2−300 K range and a 0.3 kOe applied magnetic field is displayed in Figure 10 as χ vs T and χT vs T. The χT product decreases slightly between 300 and 70 K. This decrease is related to the spin−orbit coupling effect well documented in the case of octahedral iron(II). A magnetic phase transition occurs at 25 K resulting in a χT maximum of 21.26 emu mol^{-1} K. Magnetization measurements performed up to 55 kOe show that, in the paramagnetic region ($T > 25$ K), the magnetization varies linearly with the applied magnetic field up to *ca.* 15 kOe. At 4.2 K, the field dependence of the magnetization departs from linearity above 2 kOe, but saturation is not reached, even at 55 kOe (Figure 11). When the magnetic field is cycled between 55 and −55 kOe, a characteristic hysteresis loop is obtained with a remanent magnetization of 0.17 μ_B and a coercive field of 2 kOe (Figure 11). These results clearly show that (i) the saturation of the magnetization occurs at a value lower than 1 μ_B, far away from the theoretical value for a $S = 2$ spin system (4 μ_B); (ii) the net magnetic moment at zero-field agrees with a canted spin structure; (iii) the high coercive field observed is among the largest for a molecular material. Finally, these observations agree with the presence of a weak ferromagnetic ground state resulting from the 3D ordering of this homometallic lattice as indicated by the Zeeman spectra obtained by Mössbauer spectroscopy (Figure 8b).

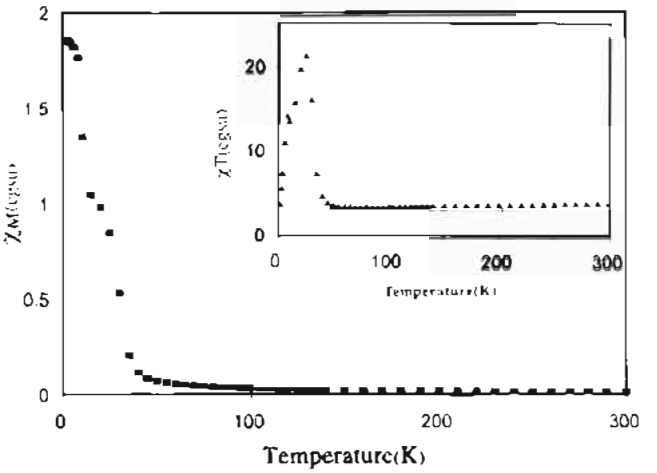

Figure 10. Variation of the magnetic susceptibility and χT product (insert) of a powdered sample of $\{Fe^{II}(bim)\}_n$ (**4**) with temperature at 0.3 kOe.

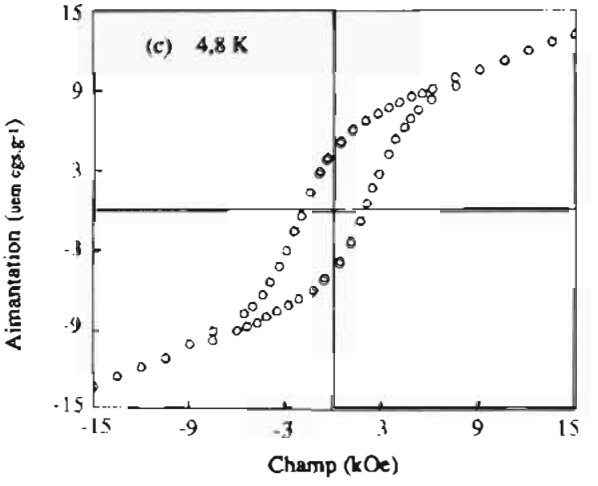

Figure 11. Field dependence of the magnetization of a powdered sample of $\{Fe^{II}(bim)\}_n$ (**4**) at 4.2 K.

Structural Hypothesis for Complex 4. On the grounds of the analytical, IR, Mössbauer spectroscopy and magnetic susceptibility results previously described, a 2D homometallic lattice in which each iron atom is linked to three nearest iron neighbors through bim^{2-} dianions as illustrated in Figure 12 can be suggested. Indeed, the analytical results and infrared spectra obtained for **4** clearly evidence the presence of Fe^{II}(bim) units. Consequently, it can be considered that the coordination sphere of each iron(II) involves three chelated bim^{2-} dianions. Furthermore, the Mössbauer data confirm a N_6 ligand environment and reveal a magnetic phase transition which implies a polymeric structure for this complex. The magnetic properties indicate the presence of a weak ferromagnetic ground state resulting from the 3D ordering of this homometallic lattice. Finally, it may be assumed that interactions between the magnetic layers corresponding to the 2D lattice of Fe^{II}(bim) molecules through hydrogen bonds involving the methanol molecules and nitrogen atoms of the bim^{2-} bridging ligands (IR section) promote the 3D ferromagnetic ordering observed.

Concluding Remarks

Complex **1** is the first example of structurally characterized mononuclear ferrous compound including two bidentate $bimH_2$ and two monodentate oxygenated ligands affording a N_4O_2

(55) (a) Richardson, H. W.; Hatfield, W. E. *J. Am. Chem. Soc.* **1976**, *98*, 835. (b) Felthouse, T. R.; Hendrickson, D. N. *Inorg. Chem.* **1978**, *17*, 2636. (c) Kolks, G.; Lippard, S. J.; Waszczak, J. V.; Lilienthal, H. R. *J. Am. Chem. Soc.* **1982**, *104*, 717. (d) Bencini, A.; Benelli, C.; Gatteschi, D.; Zanchini, C. *Inorg. Chem.* **1986**, *25*, 398.

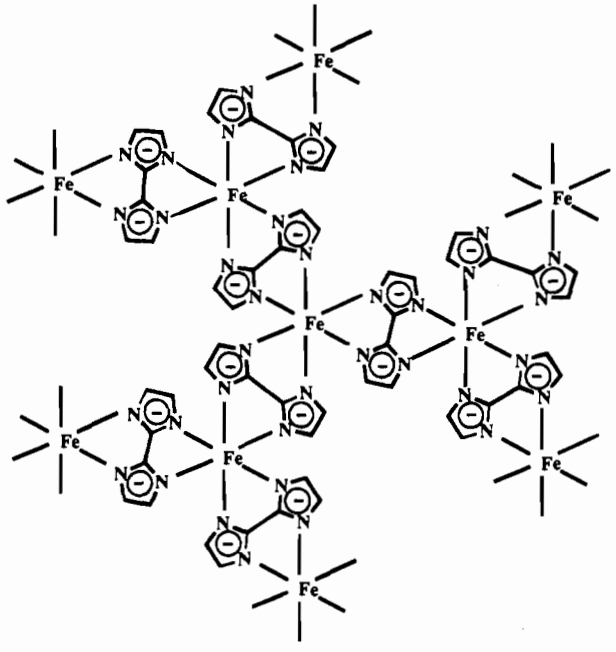

Figure 12. Schematic drawing of the structural arrangement suggested for $\{Fe^{II}(bim)\}_n$ (**4**).

coordination sphere to high−spin iron(II). The oxygen donors and $bimH_2$ ligands are trans to each other, respectively, affording a coordination octahedron compressed along the O···O axis. Comparison of the Mössbauer parameters clearly shows that a N_4O_2 ligand environment with trans oxygen donors does not afford a satisfactory modeling of the N_4O_2 ligand environment in photosynthetic non-heme ferrous sites.

Synthesis of complex **2** from $Fe^{II}(bimH_2)_2(HCOO)_2$ and CO_3-HNa shows that formate anions are readily displaced from the iron(II) coordination sphere as shown for the non-heme iron-(II) of PS 2.[7b,e] However, the suspected four imidazole and one bicarbonate coordination sphere of this natural ferrous site could not be modeled through this type of reaction due to stabilization of the bicarbonate moiety as a carbonate dianion out of the iron(II) coordination sphere. This probably results from the particularly high stability of the $[Fe^{II}(bimH_2)_3]^{+2}$ tris-chelate cation which furthermore bears six external NH functions prone to participate in an extended hydrogen bond network with the surrounding carbonate dianions. Syntheses directed at obtaining $Fe^{II}(bimR_2)_2(RCO_2)_2$ complexes including N-substituted biimidazole ligands are under way, with the goal to carry out the same type of methathesis reactions and thus explore the possibility to stabilize bicarbonate or carbonate anions in the iron(II) coordination sphere.

$[Fe^{II}(bimH)_2]_n$ (**3**) affords the first example of bridging biimidazolate monoanion. It corresponds to the non-previously described coordination mode (C) depicted in Figure 1.

All previously described complexes in which bim^{2-} exhibits the bridging (D) coordination mode depicted in Figure 1 are binuclear; $\{Fe^{II}(bim)\}_n$ (**4**), is thus the first inorganic polymeric material including the bim^{2-} dianion as a tetradentate bridging ligand. The Mössbauer and magnetic properties of **4** indicate the presence of a weak ferromagnetic ground state resulting from the 3D ordering of this homometallic lattice below 25 K.

Finally, we shall mention that **3** and **4** are the first examples of iron compounds including the biimidazolate monoanion, $bimH^-$, and dianion, bim^{2-}, respectively.

Acknowledgment. Acknowledgements are due to Dr. M. Verelst for independently checking some of the preparations described in this paper. The CNRS and the National Hellenic Research Foundation are acknowledged for partial support of this work through the CNRS/NHRF exchange program. M.A.M.L. thanks the Commission of European Communities (Science Program) for a doctoral fellowship.

Supporting Information Available: Listings of complete crystal data and experimental details, non-hydrogen atoms positional and thermal parameters, hydrogen atomic positional and thermal parameters, components of the anisotropic temperature factors, bond lengths and angles, least-squares planes and deviations of atoms therefrom, and geometry of the Fe coordination octahedra for complexes **1**, **2**, and **3**, figures showing a view of the unit cell of complexes **1**, **2**, and **3**, figures showing least-squares fitted Mössbauer spectra of complexes **1**−**3**, and listings of detailed data resulting from the magnetic susceptibility measurements for complex **4** in the 300−2 K temperature range (34 pages). Ordering information is given on any current masthead page.

IC9503242